# INSTITUTE FOR FUSION STUDIES

DOE/ET-53088-412 IFSR #412

## Nonlinear Excitation of Magnetic Undular Instability by Convective Motion

*M. Kaisig, T. Tajima, K. Shibata,* S. Nozawa,** and R. Matsumoto***
Institute for Fusion Studies
The University of Texas at Austin
Austin, Texas 78712

December 1989

* *Department of Earth Sciences, Aichi University of Education, Kariya, Aichi 448, Japan*
** *Department of Information Science, College of Arts and Sciences, Chiba University, Chiba 260, Japan*

# THE UNIVERSITY OF TEXAS

# AUSTIN

# Nonlinear Excitation of Magnetic Undular Instability by Convective Motion

M. Kaisig,[1] T. Tajima,[1] K. Shibata,[1,2] S. Nozawa[2] and R. Matsumoto[3]

20 November 1989

[1] Department of Physics and Institute for Fusion Studies, University of Texas, Austin, TX 78712

[2] Department of Earth Sciences, Aichi University of Education, Kariya, Aichi 448, Japan

[3] Department of Information Science, College of Arts and Sciences, Chiba University, Chiba 260, Japan

Headings: Nonlinear Magnetic Buoyancy Instability

## Abstract

The influence of convective motions on the evolution of the undular mode of magnetic buoyancy (the Parker instability) of an isolated horizontal flux sheet in the solar atmosphere is studied. The flux sheet is embedded in a two-temperature layer atmosphere (solar photosphere/chromosphere and its overlying much hotter corona) with a convection zone underneath. The atmosphere is assumed to be stratified under a constant gravitational acceleration. Convective motions considered are horizontal photospheric shear flows and vertical velocity fluctuations in the convectively unstable layer below the photosphere. The evolution is numerically studied in a two-dimensional space by using a 2.5-dimensional code of ideal magnetohydrodynamics.

Even if the initial magnetic flux sheet is stable to the Parker instability $\gamma > \gamma_c$, where $\gamma$ is the gas constant, or not, the horizontal velocity shear causes destabilization and drives the expansion of magnetic flux into the corona. As the instability develops, the gas slides down the expanding loop and the evacuated loop rises as a result of the enhanced magnetic buoyancy, which is similar to the nonlinear evolution of a flux loop that was originally linearly Parker unstable. Other signatures such as shock waves in the downflow region, self-similar loop expansion, etc., are also similar. Vertical velocity fluctuations in the underlying convection zone also lead to destabilization as long as the initial flux is localized within or just above the convectively unstable layer. If the initial flux is embedded in the higher layer, however, convective motions are not able to excite the Parker instability. Application to active region prominence is briefly discussed.

Subject headings: hydromagnetics - instabilities - plasmas - Sun: atmosphere - Sun: chromosphere

## I. Introduction

It is widely believed that much of the activity on the Sun such as flares, prominences, corona and mass ejections are caused by strong magnetic fields. Magnetic buoyancy plays a major role in the occurrence of these various magnetic phenomena because magnetic fields created by the dynamo action are transported from the solar interior to the surface by the magnetic buoyancy.

The "Parker instability" (Parker 1966, 1969, 1979) is an ideal magnetohydrodynamic instability driven by magnetic buoyancy. It is believed to be closely related to

the formation of interstellar clouds (e.g. Shu 1974; Mouschovias, Shu and Woodward 1974; Zweibel and Kulsrud 1975; Elmegreen 1982), and radio lobes in disk galaxies (e.g., Sofue, Fujimoto and Tosa 1976; Asséo *et al.* 1978; Duric *et al.* 1983), the escape of magnetic flux from accretion disks (e.g., Shakura and Sunyaev 1973; Stella and Rosner 1984; Kato and Horiuchi 1985, 1986), and the rise and emergence of magnetic flux tubes in the Sun and stars (e.g., Acheson 1979; Schüssler 1980; Spruit and van Ballegooijen 1982; Schmitt and Rosner 1983; Moreno-Insertis 1986; Hughes and Proctor 1988).

Since the pioneering work by Parker(1966), many authors have studied the nature of the instability under various aspects (Acheson 1979; Gilman 1970; Shu 1974). Recently Horiuchi *et al.* (1988) analyzed linear stability of a magnetized gas disk rotating around a gravitating center. The nonlinear time evolution of the Parker unstable modes for an isothermal magnetostatic gas layer in a nonuniform gravitational field were studied by Matsumoto *et al.* (1988). Shibata *et al.* (1989a) examined the nonlinear evolution of the instability in an isolated horizontal magnetic flux sheet embedded in a two-temperature layer atmosphere by using a two-dimensional magnetohydrodynamic code. The relation to emerging magnetic flux in active regions of the solar atmosphere was discussed by Shibata *et al.* (1989b).

All these numerical simulations mentioned above have assumed a small gas adiabatic constant $\gamma$ ($\gamma \approx 1.05$) in order to satisfy the linear Parker instability condition

$$\gamma < \gamma_c = 1 + \frac{1}{\beta}$$

at the beginning of the computer run, where $\beta$ is the plasma beta, the ratio of the plasma pressure to the magnetic one. The linear stability analysis (Parker 1966, 1979; Horiuchi *et al.*, 1988) shows that the Parker instability is suppressed for larger $\gamma$. In fact, the isolated magnetic flux studied by Shibata *et al.* (1989a) is stable to the Parker instability for $\gamma > 1.38$. This raises the question whether and how emerging flux in the upper photosphere and chromosphere, where $\gamma$ is likely to be about 5/3, becomes unstable and is able to expand into the corona.

In the present investigation we study by numerical simulation the influence of convective motions on the stability of a Parker *stable* magnetic flux sheet. The aim of this work is to study the general characteristics of the Parker instability with convective motions in the nonlinear stage and to examine if a destabilization of stable flux can be realized by either horizontal photospheric shearing motions and/or by vertical convective flows.

In §II we describe the assumptions made for the numerical simulations, and the basic equations. Section III presents the numerical results concerning the destabilization of a magnetic flux sheet by the photospheric velocity shear. In §IV we study the destabilization by convective motions. Finally, §V is devoted to the summary and discussion.

## II. Basic equations and numerical methods

### a) Assumptions and Basic Equations

We made the following assumptions for our numerical simulations: (1) the medium is an ideal gas, (2) the gas is a polytrope of index $\gamma$, (3) the magnetic field is frozen in the gas, (4) the gravitational acceleration is constant. Cartesian coordinates $(x, y, z)$ are adopted so that the z-direction is antiparallel to the gravitational acceleration. It is assumed that the evolution is two-dimensional with $\partial/\partial y = 0$, but $B_y$ and $V_y$ not zero. Thus the basic equations are as follows:

$$\frac{\partial \rho}{\partial t} + \frac{\partial}{\partial x}(\rho V_x) + \frac{\partial}{\partial z}(\rho V_z) = 0, \tag{1}$$

$$\frac{\partial}{\partial t}(\rho V_x) + \frac{\partial}{\partial x}\left[\rho {V_x}^2 + p + \frac{1}{8\pi}({B_y}^2 + {B_z}^2 - {B_x}^2)\right] + \frac{\partial}{\partial z}\left(\rho V_x V_z - \frac{B_x B_z}{4\pi}\right) = 0, \tag{2}$$

$$\frac{\partial}{\partial t}(\rho V_y) + \frac{\partial}{\partial x}\left(\rho V_y V_x - \frac{B_x B_y}{4\pi}\right) + \frac{\partial}{\partial z}\left(\rho V_y V_z - \frac{B_y B_z}{4\pi}\right) = 0, \tag{3}$$

$$\frac{\partial}{\partial t}(\rho V_z) + \frac{\partial}{\partial x}\left[\rho V_z V_x - \frac{B_x B_z}{4\pi}\right] + \frac{\partial}{\partial z}\left[\rho {V_z}^2 + p + \frac{1}{8\pi}({B_x}^2 + {B_y}^2 - {B_z}^2)\right] + \rho g = 0, \tag{4}$$

$$\frac{\partial B_x}{\partial t} + \frac{\partial}{\partial z}(V_z B_x - V_x B_z) = 0, \tag{5}$$

$$\frac{\partial B_y}{\partial t} + \frac{\partial}{\partial x}(V_x B_y - V_y B_x) + \frac{\partial}{\partial z}(V_z B_y - V_y B_z) = 0, \tag{6}$$

$$\frac{\partial B_z}{\partial t} + \frac{\partial}{\partial x}(V_x B_z - V_z B_x) = 0, \tag{7}$$

$$\begin{aligned}
&\frac{\partial}{\partial t}\left[\frac{p}{\gamma - 1} + \frac{1}{2}\rho({V_x}^2 + {V_y}^2 + {V_z}^2) + \frac{1}{8\pi}({B_x}^2 + {B_y}^2 + {B_z}^2)\right] \\
&+ \frac{\partial}{\partial x}\left[\frac{\gamma}{\gamma - 1}\rho V_x + \frac{1}{2}\rho V_x({V_x}^2 + {V_y}^2 + {V_z}^2) + \frac{B_z}{4\pi}(V_x B_z - V_z B_x) + \frac{B_y}{4\pi}(V_x B_y - V_y B_x)\right] \\
&+ \frac{\partial}{\partial z}\left[\frac{\gamma}{\gamma - 1}\rho V_z + \frac{1}{2}\rho V_z({V_x}^2 + {V_y}^2 + {V_z}^2) - \frac{B_x}{4\pi}(V_z B_x - V_x B_z) + \frac{B_y}{4\pi}(V_z B_y - V_y B_z)\right] \\
&- \rho g V_z = 0,
\end{aligned} \tag{8}$$

where g is the gravitational acceleration and other symbols have their usual meaning.

b) Initial conditions

We consider a two-temperature layered atmosphere which is regarded as a simplified abstraction of the Sun's photosphere/chromosphere and its overlying much hotter corona. Hereafter we call the hot layer the corona, the lower part of the cold layer the photosphere and the higher part of the cold layer the chromosphere, but never specify the exact height of transition between the photosphere and the chromosphere. The distribution of the initial temperature is assumed to be

$$T(z) = T_{ch} + (T_{cor} - T_{ch}) \cdot \frac{1}{2}\left[tanh\left(\frac{z - Z_{cor}}{w_{tr}}\right) + 1\right], \tag{9}$$

where $T_{cor}/T_{ch}$ is the ratio of the temperature in the corona to that in the chromosphere, $Z_{cor}$ is the height of the base of the corona and $w_{tr}$ is the temperature scale height in the transition region. For all our calculations we assumed $T_{cor}/T_{ch} = 25$, $Z_{cor} = 18H$ and $w_{tr} = 0.6H$, where H is the pressure scale height of the chromosphere.

We assume that the magnetic field is initially parallel to the x-axis $\vec{B} = (B(z), 0, 0)$. The distribution of magnetic field strength B(z) is given by

$$B(z) = [8\pi p(z)/\beta(z)]^{1/2}, \tag{10}$$

where

$$\beta(z) = \beta_0/f(z), \tag{11}$$

$$f(z) = \frac{1}{4}\left[tanh\left(\frac{z - z_0}{w_0}\right) + 1\right]\left[-tanh\left(\frac{z - z_1}{w_1}\right) + 1\right], \tag{12}$$

and where $\beta_0$ is the ratio of the gas pressure to magnetic pressure at the center of the magnetic flux sheet, $z_0$ and $z_1 = z_0 + D$ are the heights of the lower and upper boundary of the magnetic flux sheet, D is the vertical thickness of the flux sheet, and $w_0$ and $w_1$ are the scale heights of the magnetic flux sheet at the lower and upper boundary.

The initial density and pressure distributions are numerically calculated by using equations (10) and (11) and the equation of magnetostatic equilibrium

$$\frac{d}{dz}\left[p + \frac{B^2(z)}{8\pi}\right] - \rho g = 0. \tag{13}$$

c) Boundary conditions

We assume symmetric boundaries for $x = 0$, $x = X_{max}$ and $z = 0$, and a free boundary for $z = Z_{max}$ (see Shibata 1983). In order to check the effect of the free boundary at $z = Z_{max}$, we also simulated the case with an absorbing layer (Sato and Hayashi 1979) between $z = Z_{max}$ and the numerically true boundary at $z = Z_{max} + z_A$. Wave reflection and unphysical inflow at the free boundary are quickly damped out in the absorbing layer. This enables us to distinguish between numerical and true physical effects.

Equations (1) - (8) are nondimensionalized by using the following normalizing constants: H the scale height of the chromosphere, $C_s$ the sound velocity in the photosphere, and $\rho_0$ the density at the base of the atmosphere (z=0). Equations (1) - (8) are solved numerically by using a modified Lax-Wendroff scheme (Rubin and Burstein 1967) with an artificial viscosity according to Richtmyer and Morton (1967). The tests and accuracy of such a MHD code have been described by Shibata (1983), Shibata and Uchida (1985), Matsumoto *et al.* (1988), Umemura it et al. (1988), and Tajima (1989). The mesh sizes are $\Delta z = 0.15$ for $z < Z_{cor}$ and slowly increasing for $z \geq Z_{cor}$, $\Delta x = X_{max}/(N_x - 1)$, where $N_x$ is the number of mesh points in the x-direction. The total number of mesh points is $(N_x \times N_z) = (101 \times 172)$, the total area is $(X_{max} \times Z_{max}) = (80 \times 35)$ in a typical model in units of the pressure scale height.

## III. Nonlinear destabilization by horizontal velocity shear

We assume that the magnetic field is initially localized in the chromosphere with $z_0 = 4H$, $D = 4H$ and $w_0 = w_1 = 0.5H$. Small velocity perturbations of the form

$$V_x = Af(z)\sin\left[\frac{2\pi(x - X_{max}/2)}{\lambda}\right] \tag{14}$$

are initially imposed on the magnetic flux sheet ($z_0 < z < z_1$) within the finite horizontal domain ($X_{max}/2 - \lambda/2 < x < X_{max}/2 - \lambda/2$), where $\lambda$ is the horizontal wavelength of the velocity perturbations, $X_{max}$ is the horizontal size of the computational domain, and A is the amplitude of the initial perturbation. In our calculations we assume $X_{max} = 80H$ and $\lambda = 20H$. This perturbation is not exactly an unstable eigenfunction of the Parker instability (Horiuchi *et al.* 1988), but the growth rate of

the perturbation in the linear regime agrees well with that obtained from the exact linear analysis (Shibata *et al.* 1989a).

Furthermore, we assume shearing motions in the photosphere ($z < Z_{cor}$) of the form

$$V_y(x) = V_{y0} \cdot \tanh\left(\frac{x - X_{max}/2}{w_{sh}}\right) \tag{15}$$

where $V_{y0}$ is the amplitude of the shear flow and $w_{sh}$ is the horizontal width of the shearing region. Note that we assume the shearing motion as an initial condition and that we solve the equation of motion in y-direction. Hence the shear flow is decelerated by the magnetic torque as time proceeds, so that the kinetic energy decreases with time as shown in Fig. 4.

a) Effect of shearing motions on the Parker instability

In this subsection, we describe the influence of photospheric shearing motions on the overall evolution of the Parker instability. The parameters of this model are as follows: $\gamma = 1.05$, $\beta_0 = 1.0$ and $A = 0.05$. These parameters are identical with model 3 of Shibata *et al.* (1989a) and provide the Parker mode linearly unstable even without shear motions. The additional shear flow is characterized by $V_{y0} = 0.9C_s$ and $w_{sh} = 8H$ (Eq. 15). Compared to observations (Brants and Steenbeck 1985; Zwaan 1985), which show shearing motions up to $0.6km/s$, the magnitude of the shear flow is too large to be realistic. However, simulations with different $V_{y0}$ show that the amplitude of the shear flow does not qualitatively affect the overall evolution. Its quantitative effect is: the smaller $V_{y0}$ is, the larger is the computational time. Hence, this value of $V_{y0}$ is chosen simply for computational convenience.

Figure 1 shows the time variations of the magnetic field lines $(B_x, B_z)$, the velocity field $(V_x, V_z)$, and the density distribution $(\log \rho)$. As the instability develops, the magnetic flux bows out of the photosphere and forms a loop. The magnetic loop quickly expands into the corona, increasing its effective wavelength with time. The initially unperturbed part of the magnetic flux sheet is also disturbed by the influence of the instability in the perturbed part ($X_{max}/2 - \lambda/2 < x < X_{max}/2 + \lambda/2$). Thus magnetic flux in the initially unperturbed part also expands because of the Parker instability and forms two minor side loops seen in Fig. 1. The gas slides down the expanding loop and the evacuated loop rises as a result of the enhanced magnetic buoyancy. Dense regions are created in the valleys of the undulating field lines, whereas rarefied regions are formed around the top of the magnetic loop. Shock

waves are produced in the downflow near the footpoints of the loop when the downflow velocity exceeds the local speed of sound. These characteristics are the same as in the nonlinear simulations of Matsumoto *et al.* (1988) in the case of an isothermal atmosphere under a nonuniform gravitational field, and as in the calculations of Shibata *et al.* (1989a).

Figure 2 shows the one-dimensional z-distribution of the vertical velocity ($V_z$), the local Alfvén speed ($V_a$), the magnetic field strength ($\log B_x$) and ($\log B_y$), the density ($\log \rho$), and the ratio of the magnetic pressure to the gas pressure (= the inverse of the local plasma $\beta$) at $x = X_{max}/2$ (middle of the magnetic loop). In the nonlinear regime, both the rise velocity of the loop and the local Alfvén speed at the top of the loop increase linearly with height and show a self similar behaviour with height, as noted recently by Shibata *et al.* (1989a). As the loop rises, the local Alfvén speed increases as a result of the evacuation by the downflow along the loop, and hence the local $\beta$ decreases significantly. The z-distribution of the density $\rho$ and the magnetic field strength $B_x$ below the top of the loop tend to a steady state distribution, with

$$\rho \propto \Delta z^{-4} \qquad (16)$$

and

$$B_x \propto \Delta z^{-1}, \qquad (17)$$

where $\Delta z = z - z_0$ and $z_0 = 4.0$. This magnetic field distribution corresponds to that of a current-free (force-free) one and is essentially the same as that found in previous papers (Shibata *et al.* 1989a,b).

Compared to the simulations of Shibata *et al.* (1989a), the present results show that the inclusion of photospheric shearing motions does not drastically modify the overall characteristics of the Parker instability and that it quantitatively influences the time scale of the evolution and the length of the loop. That is, the time scale is shortened and the spatial scale is enlarged in the present case. At time $t = 43$ the velocity of the rising loop is about 1.15 in units of the initial sound speed in the chromosphere, while it was about 0.6 in the case without shearing motions (Shibata *et al.* 1989a). The level of ($\log B_x = -2.0$) reaches a height of $z = 30H$ at time $t = 43$ compared to $z = 20H$, and the maximum downflow velocity at $t = 47$ is 5.8 compared to 3.8 at $t = 51$ in the case without photospheric shear flows. The distance between the footpoints of the magnetic field amounts to $50H$ at $t = 40$ in the x,z-plane, which corresponds to a real distance of $87H$ in three dimensions due to

the amplitude of $0.9C_s$ of the shear flow, compared to a distance of $30H$ at $t = 51.4$ in the simulations of Shibata *et al.* (1989a) without shear flow. The maximum value of $V_y$ in the upper chromosphere is $3.7C_s$ at $t = 55$.

At the same time, the results show that shear flows do not significantly increase the stored magnetic field energy when the Parker instability is permitted. Even when the shear flow is applied, the induced magnetic buoyancy instability takes place more quickly and thus the energy release is faster. This should be compared with the case of Steinolfson and Tajima (1987), in which the stored magnetic energy kept increasing, as no instability was permitted because of geometry. In the case of Zaidman and Tajima (1989), instead of the Parker instability, the twist-kink instability was permitted as the magnetic energy was being stored through shear flows. In this case the stored magnetic energy did not significantly increase, similar to the present case.

b) Effect of shearing motions on Parker stable flux sheet

We now study the case where the magnetic flux sheet is *linearly stable* with respect to the Parker (undular) mode because of larger $\gamma$ ($= 1.5$), where $\gamma_c = 1 + \frac{1}{\beta}$ is 1.38 and $\gamma > \gamma_c$. However, we shall show that the Parker mode becomes *nonlinearly* unstable due to shearing motions we apply. We assume $A = 0$. Other parameters are the same as in subsection IIIa.

Figure 3 shows the magnetic field configuration $(B_x, B_z)$ of our simulations. Significantly, we still witness the buoyant loop expansion in spite of its linear Parker stability. The morphology of this case in Fig. 3 is similar to that of the Parker unstable case in Fig. 1, besides the fact that no minor side loops are formed. This is because the present magnetic flux sheet is stable to the Parker instability. The expansion of the loop is caused by the increase of magnetic pressure as a result of the shearing of the magnetic field lines. In this case the increased storage of magnetic field energy by shearing motions is similar to the cases of Steinolfson and Tajima (1987) and Zaidman and Tajima (1989). The self-similar and exponential time evolution of expanding loop is again observed. This then should be called nonlinear destabilization of the undular mode by shear flow. The size of the loop and the rise velocities are somewhat smaller than those of the linearly unstable case studied in section IIIa. The maximum value of $V_y$ in the upper chromosphere is $3.7C_s$ at $t = 55$.

Figure 4 shows the time variation of magnetic, gravitational, thermal and kinetic energies in the system. It should be noted that $\Delta E = E(t) - E(0)$ and that the magnetic energy ($E_m$) is normalized to its initial value. The magnetic ($E_m$) and

gravitational ($\Delta E_g$) energies slightly increase within the first 30 timescales, while the kinetic ($\Delta E_k$) and thermal ($\Delta E_{th}$) energies decrease. The increase in magnetic energy is due to the amplification of the magnetic field by the photospheric shear flow and the decrease in kinetic energy mainly due to the deceleration of the shearing motions. After this first period ($t \approx 30$) the magnetic field quickly expands upward and reduces its energy. Most of the released energy is converted into thermal energy through compressional and shock heating. The total energy in the simulation is conserved within 1% of its initial value.

c) Dependence of horizontal wavelength

The dependence of the evolution of an isolated magnetic flux sheet on the horizontal wavelength of the velocity shear is investigated. The initial flux is assumed to be stable to the Parker instability. We used the following parameters: $\gamma = 1.5$, $X_{max} = 160H$ (twice the previous cases) and $V_{y0} = 3.6C_s$, $w_{sh} = 32H$ to ensure the same shear rate as in our previous models (IIIa and IIIb).

The numerical results are displayed in Fig. 5. The expansion of the flux is quite different from the former cases discussed in section IIIb. As the instability develops, the horizontal size of the loop remains nearly constant in the vertical direction, without exhibiting self-similarity anymore. The flow pattern is characterized by the mainly horizontal velocities. No shock waves are produced at the footpoints. In Fig. 6 we display the one-dimensional distribution of the vertical velocity ($V_z$), the local Alfvén speed ($V_a$), the magnetic field strength ($\log B_x, \log B_y$) and the density ($\log \rho$) at ($x = X_{max}/2$). Figure 6 shows that in this case the top of the loop is only slightly evacuated, thereby keeping the Alfvén speed and the rise velocity low and nearly constant as the flux sheet expands into the corona. Note the significant differences between Figs. 2b and 6b and also differences between Figs. 2d and 6c.

We see from Figs. 6c and 6d that the magnetic field strength $B_y$ and the density $\rho$ decrease exponentially with height. The approximate relations in the numerical results, shown by the dashed lines in Figs. 6c and 6d, are

$$B_y \propto \exp(-z/H_m), \tag{18}$$

$$\rho \propto \exp(-z/H_\rho), \tag{19}$$

with $H_m \cong 8.0H$ and $H_\rho \cong 4.6H$. Furthermore, we see from Fig. 6b that the Alfvén speed $V_a$ is nearly constant. Since $B_x \ll B_y$, this requires that $B_y/\sqrt{\rho} \cong const.$

or $H_m \cong 2H_\rho$, which agrees roughly with our numerical results. The value of $H_\rho$ can be made plausible if we assume hydrostatic equilibrium in the vertical direction (remember that $V_z \leq 0.3C_s$). Under the assumption that $V_a = const.$, we find from equation (13) $H_\rho = (1 + 1/\beta)H$, which gives for a typical value of $\beta$ ($1/\beta = 4.0$, see Fig. 2f) $H_\rho = 5H$, in agreement with our numerical results. This shows that in the case of long wavelength perturbations the magnetic flux sheet expands under nearly hydrostatic equilibrium into the corona. This is in contrast to the expansion with approximate current-free equilibrium in the case of short wavelength (Figs. 1 and 2).

## IV Nonlinear destabilization by convective motions

In contrast to the simulations of section III in which the flow was horizontal (in the y-direction) we now allow a convectively unstable region beneath the photosphere/chromosphere as a model of the solar convection zone. This allows more self-consistent and dynamical coupling between the convection zone and the solar atmosphere.

The initial temperature distribution in the convection zone is assumed to be

$$T(z) = T_{ch} - az|dT/dz|_{ad} \tag{20}$$

for $z_c \leq z \leq 0$, where z is the height measured from the base of the photosphere, $z_c$ is the base height of the convection zone, $|dT/dz|_{ad} = [(\gamma - 1)/\gamma](T_{ch}/H)$ is the adiabatic temperature gradient and $a$ is a numerical constant of the order of unity. For numerical reasons, we adopt $z_c = -5H$ and $a = 2$. Although these values are not realistic for actual solar convection zone (e.g., Spruit 1974), these are sufficient to study the fundamental nonlinear interaction between the magnetic field and convection just below the photosphere (Shibata *et al.* 1989c).

In order to start the instability in the convectively unstable layer, small vertical velocity perturbations (with an amplitude of 0.01 in units of the speed of sound) are imposed initially on the magnetic flux sheet within the finite horizontal domain ($X_{max}/2 - \lambda/4 < x < X_{max}/2 + \lambda/4$), where $\lambda = 14H (\simeq 3000km)$. This perturbation is not exactly an unstable eigenfunction. However, the growth rate of the perturbation in the linear regime agrees well with that obtained from the exact linear analysis (see Fig. 8 below).

The magnetic field is initially horizontal and is localized in $z_0 \leq z \leq z_0 + D$ (see Eqs. (11) and (12)). The distribution of the magnetic field strength is given by Eq.

(10), where we take $\beta_0 = 4.0$ and $D = 2H$ for the vertical thickness of the flux sheet. We study three different locations of the initial magnetic flux: within the convection zone just below the photosphere ($z_0 = -2H$), on top of the convection zone ($z_0 = 0$) and within the chromosphere ($z_0 = 5H$). The parameters are as follows: $\gamma = 5/3$, $Z_{max} = 42H$, $Z_{cor} = 13H$. As in the case of the previous section IIIb, the magnetic flux with $z_0 > 0$ is stable against the Parker mode because of large $\gamma(= 5/3)$.

a) The nature of convective motions

We carry out linear analysis of the convective instability with and without magnetic flux. Figure 7 shows the linear growth rates of the convective instability as a function of the horizontal wavenumber for different plasma $\beta$ (see Nozawa *et al.* 1989, for details on the linear stability analysis for the system of Eqs. (1) - (12) and (20)). We study two cases. In the first case (Fig. 7a) the magnetic flux sheet is located in the convection zone ($z_0 = -2H$, when $z_0$ is defined in Eq. (12)). In the second case (Fig. 7b) the magnetic flux sheet is above the convection zone ($z_0 = 0$). We call the first case as a partially magnetized convection zone and the second as an unmagnetized convection zone. In the latter case the growth rates increase with wavenumber $k_x$ independently of $\beta$, while in the former case a magnetic field within the convection zone stabilizes convection by magnetic tension for small wavelengths ($k_x > 0.3$) This stabilization is stronger for smaller $\beta$. For $\beta \to \infty$ the growth rates converge toward the case with $z_0 = 0$. For long wavelengths ($k_x < 0.3$) the magnetic field has destabilizing effect due to the onset of the Parker instability.

In Fig. 8 we show the time evolution of the horizontal convective velocity at $(x, z) = (44.8, 1.9)$ for the case with $z_0 = -2H$. This point $(44.8, 1.9)$ is not in the convectively unstable layer ($-5 \leq z \leq 0$). However, the eigenfunction of the convective instability has such a broad distribution extending beyond $z = 0$, so that it can be said that this point is actually in the convection zone. The dashed line represents the result of the linear analysis of the convective instablility, and corresponds to the growth rate of the most unstable eigenmode. The solid line shows the evolution of the convective instability in our numerical simulation. In the period between $t = 10$ and $t = 50$ the numerical calculations fit the linear behavior well. Nonlinear saturation sets in at about $t \approx 50$. The strong increase within the first 5 timescales is due to the fact that the convective instability is initiated by vertical velocity perturbations.

b) Overall evolution

First we discuss the case with $z_0 = -2H$: The magnetic flux sheet is initially located in the convection zone. Figure 9 shows typical results for the magnetic field lines. The magnetic flux is first carried by the convective and magnetic buoyancy forces from the convection zone toward the photosphere ($t \approx 50\tau \approx 18min$). As the loop expands into the chromosphere and corona, it shows the same self-similar behavior as in our previous case of the Parker unstable magnetic flux sheet (section IIIb). The magnetic field configuration below the photosphere is dominated by the convective motions and forms a cellular structure (Figs. 9b and 9c). As the velocity fluctuations expand within the convection zone, the initially unperturbed part of the magnetic flux sheet is also disturbed. Thus the flux in the initially unperturbed part also expands and forms two minor side loops. Shock waves are formed in the downflow.

Figure 10 shows the results with $z_0 = 0$: The magnetic flux sheet is initially located just above the convectively unstable layer. In the course of evolution, magnetic flux is partially transported by convection into the region below the photosphere. The upward motion of the gas in the nonlinear regime of the order of $0.2C_s$, overshooting from the convection zone into the photosphere, transports the magnetic flux sheet upwards. The gas slides down from the top of the expanding loop along the field lines. The evacuated loop rises as a result of enhanced magnetic buoyancy. As the loop expands into the corona, its overall shape is similar to the case where the destabilization is driven by velocity shear (sec. III).

The case where the magnetic flux is intially embedded in the higher atmospheric layer ($z_0 = 5H$) than in the previous calculations is similar to the model studied by Shibata *et al.* (1989a), except for the fact that here we examine a stable magnetic field configuration and include a convection zone. The convective disturbances initiated from below the photosphere propagate upwards in the form of magnetohydrodynamic waves, but are not able to destabilize the flux sheet in the upper chromosphere. This is not a stabilizing effect of the overlying corona, since simulations with different heights of the coronal base ($Z_{cor}$) show the same behavior.

The results of the overall evolution are summarized in Table 1, including the behaviour of additional cases. This table displays the stability properties for different plasma $\beta$ and different locations $z_0$ of the lower base of the initial magnetic flux sheet. It clearly shows that magnetic flux within the convection zone or just above easily becomes unstable by convective motions. On the other hand, destabilization for

magnetic flux in the chromosphere occurs only for low $\beta$ ($\beta \approx 1$), since the growth rate of the Parker instability of isolated magnetic flux increases with decreasing $\beta$.

## V. Summary and Discussion

In this investigation we have presented results of numerical simulations of the nonlinear evolution of the Parker instability in an isolated horizontal magnetic flux sheet which is subject to convective motions. We have considered convective motions in the form of horizontal photospheric shear flows as well as vertical velocity fluctuations in a convectively unstable layer below the photosphere.

The most important results of our investigation can be summarized as follows. Even if the initial flux is stable with respect to the Parker (undular) mode, both velocity shear and fluctuations in a convection zone are capable of nonlinearly driving the instability and resulting expansion of magnetic flux into the corona. In the nonlinear regime, the overall evolution is characterized by the self-similar expansion much like the previous studies (Shibata *et al.* 1989a,b), where initial flux is in a layer unstable to the Parker mode. Photospheric shear flows do not drastically affect the nonlinear expansion of magnetic flux as long as the initial flux is unstable to the Parker mode.

We thus conclude that the nonlinear expansion of magnetic flux is nearly independent of the primary excitation mechanism. This investigation has shown that convective motions can cause nonlinear destabilization and expansion of magnetic flux from the convection zone into the corona even if the solar photosphere and chromosphere may be stable against the Parker mode. When the Parker mode is stable, shear motions can convert their kinetic energy into stored magnetic energy. On the other hand, when it is unstable, this storage process has hardly enough time to take place because the Parker instability develops linearly.

The nature of destabilization can be different. In the case of velocity shear the magnetic pressure increases due to the generation of $B_y$. This causes vertical expansion of the magnetic sheet. The downflow along the field lines evacuates the gas at the top of the loop and drives the instability. If the destabilization occurs by vertical velocity fluctuations in the convection zone, the magnetic flux is pushed upwards by mechanical movements. This deforms the flux sheet and excites the instability in the same way as described above.

In the nonlinear regime, the overall evolution is often characterized by the self-similar expansion as found in the previous studies (Shibata *et al.* 1989a,b). Figure 2 shows that the Alfvén speed increases with height, but not linearly as found by Shibata *et al.* (1989a,b). The difference is due to the fact that in the present case the magnetic field curvature is nearly zero in the middle part of the loop. Therefore, the evacuation at the top of the loop is slower and thus the local Alfvén speed smaller.

Figures 1 and 3 show the existence of strong MHD shock waves near the footprints of the loops. Shocks occur since the downflow speed exceeds the local sound speed and the Alfvén speed. In MHD, three shock modes become possible (Kantrowitz and Petschek 1966; Priest 1982). They are classified according to their phase speeds as slow, intermediate, and fast. The slow shock has the effect of decreasing the magnetic field strength as it passes and making the magnetic field rotate towards the shock normal, whereas the fast shock (which speed exceeds $(C_s^2+V_a^2)^{1/2}$) has the opposite effect. A primary difference between intermediate shocks and the other two types is that the component of the magnetic field parallel to the shock plane reverses direction across an intermediate shock while it retains its direction across the others. Whereas the magnetic field strength increases across fast shocks and decreases across slow shocks, it may either increase or decrease across the intermediate shock. In our simulations we can identify a fast MHD shock in the lower region of the downflow near the footpoints of the loop and an intermediate shock in the upper region. The approximate location of shocks is indicated in Fig. 1c ($t = 40$), with solid lines representing the fast shock and dashed lines the intermediate shock.

The process of expanding magnetic flux can be regarded as a reliable model for emerging flux regions (EFR) on the Sun and can explain many basic properties of arch filament systems. When we compare numerical results with observations, we will use a photosperic pressure scale height of 200 km and a speed of sound of 10 km/s, which are typical values for the solar chromosphere and photosphere. The rise velocity of the magnetic loop predicted by numerical simulations (Figs. 2 and 4) is about 10 - 15 km/s. This value agrees well with the observed rise velocity of arch filaments (Bruzek 1967, Bruzek 1969, Chou and Zirin 1988, Tanbell *et al.* 1988). The downflow speed found in the simulations is abount 30 - 60 km/s in the chromosphere. This value is also consisitent with the observed downflow speeds (Bruzek 1969, Zwaan, Brants and Cram 1985). Our simulations show that strong shock waves are formed near the footpoints of the magnetic loop, which may be related to bright plages observed near filament systems (Bumba and Howard 1965, Born 1974).

The kinetic energy of downflow can account for a portion of the chromospheric heating (Priest 1982). According to the numerical results, the energy release due to the expansion of magnetic flux is almost entirely converted into thermal energy of the plasma through compressional and shock heating. The enhanced activities in emerging flux regions (Priest 1982) are easily understood as due to the release of magnetic energy stored in magnetic fields when the magnetic flux expands upward into the chromosphere and corona.

According to our numerical results, the time scale for the emergence of magnetic flux from the bottom of the atmosphere to the coronal level is about 20 min. This is comparable to the observed time difference between the first appearance in magnetograms and the appearance of bright plage regions (Harvey and Martin 1973).

The simulation results for very long filaments (Figs. 5 and 6) are consistent with observations of the active regions after the EFR stage. According to observations (Malherbe *et al.* 1983; Schmieder *et al.* 1985; Hanaoka and Kurokawa 1990), there are some filaments between the two magnetic polarities in this stage which are usually very long ($> 3 \times 10^4 km$) and do not show any rise motion ($V_z \ll 10 km/s$), but show large downflow velocity ($\sim 30 km/s$). The reason of no rise motion could be the deceleration by the overlying magnetic field (Shibata *et al.* 1989b). Our results present an alternative (or additional) possibility that the very small rise velocity is simply due to a great length of the filament in the presence of velocity shear, as shown in Fig. 5. The horizontal velocity of $30 - 50 km/s$ along the filament is also consistent with observations (Hanaoka and Kurokawa 1990).

General effects of magnetic shear and the network coronal magnetic fields with velocity shear will be discussed in a separate paper (Shibata *et al* 1990a).

The computations were performed on the Cray X-MP/24 at the Computer Center of the University of Texas at Austin, and on FACOM VP200 at the Institute of Plasma Physics of Nagoya University. This work was supported in part by the National Science Foundation grant ATM88-11128, and US Department of Energy DE-FG05-80ET53088. and in part by the Scientific Research Fund of the Ministry of Education, Science, and Culture(01740143).

## References

Acheson, D.J. 1979, *Solar Phys.*,**62**, 23.

Asséo, E., Cesarsky, C.J., Lachièze-Rey, M., and Pellat, R. 1978, *Ap. J. (Letters)*, **225**, L21.

Born, R. 1974, *Solar Phys.*,**38**, 127.

Brants, J.J. and Steenbeck, J.C.M. 1985, *Solar Phys.*,**96**, 229.

Bruzek, A. 1967, *Solar Phys.*,**2**, 451.

Bruzek, A. 1969, *Solar Phys.*,**8**, 29.

Bumba, V. and Howard, R. 1965 *Ap.J.*,**141**, 1492.

Chou, D. and Zirin, H. 1988, *Ap.J.*,**333**, 420.

Duric, N., Seaquist, E.R., Crane, P.C., Bignell, R.C., and Davis, L.E. 1983, *Ap. J. (Letters)*,**273**, L11.

Elmegreen, B.G. 1982, *Ap.J.*,**253**, 634.

Gilman, P.A. 1970, *Ap.J.*,**162**, 1019.

Hanaoka, Y. and Kurokawa, H. 1990, *Solar Phys.*,in press.

Harvey, K.L. and Martin, S.F. 1973, *Solar Phys.*,**32**, 389.

Horiuchi, T., Matsumoto, R., Hanawa, T., and Shibata, K. 1988, Pub. Astr. Soc. Japan, **40**, 147.

Hughes, D.W., and Proctor, M.R.E. 1988, *Ann. Rev. Fluid Mech.*, **20**, 187.

Kantrowitz, A.R. and Petschek, H.E. 1966, in *Plasma Physics in Theory and Application*, W.B. Kunkel (ed.), (New York: McGraw-Hill)

Kato, S., and Horiuchi, T. 1985, *Pub. Astr. Soc. Japan*,**37**, 399.

Kato, S., and Horiuchi, T. 1986, *Pub. Astr. Soc. Japan*,**38**, 313.

Malherbe, J.M., Schmieder, B., Ribes, E., and Mein, P. 1983, *Astr. Ap.*,**119**, 197.

Matsumoto, R., Horiuchi, T., Shibata, K., and Hanawa, T. 1988, *Pub. Astr. Soc. Japan*, **40**, 171.

Moreno-Insertis, F. 1986, *Astr. Ap.*,**166**, 291.

Mouschovias, T.Ch., Shu, F.H., and Woodward, P.R. 1974, *Astr. Ap.*,**33**, 73.

Nozawa, S., Shibata, K., Matsumoto, R., Tajima, T., and Sterling, A.C. 1989, in preparation.

Parker, E.N. 1966, *Ap.J.*,**145**, 811.

Parker, E.N. 1969, *Space Sci. Rev.*, **9**, 651.

Parker, E.N. 1979, *Cosmical Magnetic Fields* (Oxford: Clarendon Press).

Priest, E.R. 1982, *Solar Magnetohydrodynamics* (Dordrecht: Reidel)

Richtmyer, R.O., and Morton, K.W. 1967 *Difference Methods for Initial Value Problems* (2nd ed.; New York: Interscience), chap. 13.

Rubin, E., and Burstein, S.Z. 1967, *Comput. Phys.*, **2**, 178.

Sato, T. and Hayashi, T. 1979, *Phys. Fluid*, **22**, 1189.

Schmieder, B., Malherbe, J.M., Poland, A.I., and Simon, G. 1985 *Astr. Ap.*,**153**, 64.

Schmitt, J.H.M.M., and Rosner, R. 1983, *Ap.J.*,, **265**, 901.

Schüssler, M. 1980, *Astr. Ap.*,**89**, 26.

Shakura, N.I., and Sunyaev, R.A. 1973, *Astr. Ap.*,**24**, 337.

Shibata, K. 1983, *Pub. Astr. Soc. Japan*,**35**, 263.

Shibata, K., and Uchida, Y. 1985, *Pub. Astr. Soc. Japan*,**37**, 31.

Shibata, K., Tajima, T., Matsumoto, R., Horiuchi, T., Hanawa, T., Rosner, R., and Uchida, Y. 1989a, *Ap.J.*,**338**, 471.

Shibata, K., Tajima, T., Steinolfson, R.S., and Matsumoto, R. 1989b, *Ap.J.*,**345**, 584.

Shibata, K., Nozawa, S., Matsumoto, R., Sterling, A.C., and Tajima, T. 1989c, *Ap. J. (Letters)*,submitted.

Shibata, K., Kaisig, M., Tajima, T., and Matsumoto, R. 1990, in preparation.

Shu, F.H. 1974, *Astr. Ap.*,**33**, 55.

Sofue, U., Fujimoto, M., and Tosa, M. 1976, *Pub. Astr. Soc. Japan*,**28**, 317.

Spruit, H.C. 1974, *Solar Phys.*,**34**, 277.

Spruit, H.C., and van Ballegooijen, A.A. 1982, *Astr. Ap.*,**106**, 58.

Steinolfson, R.S. and Tajima, T. 1987 *Ap.J.*,**322**, 503.

Stella, L., and Rosner, R. 1983, *Ap.J.*,**277**, 312.

Tajima, T. 1989, *Computational Plasma Physics* (Addison-Wesley, Redwood City, CA).

Tarbell, T., Ferguson, S., Frank, Z., Title, A. and Topka, K. 1988, in Proc. MAX '91 Workshop (Kansas City), p. 50.

Umemura, S, Iki, K., Shibata, K., and Sofue, Y. 1988, *Pub. Astr. Soc. Japan*, 40, 25.

Zaidman, E.G. and Tajima, T. 1989, *Ap.J.*,**338**, 1139.

Zwaan, C. 1985, *Solar Phys.*,**100**, 406.

Zwaan, C., Brants, J.J., and Cram, L.E. 1985, *Solar Phys.*,**95** 3.

Zweibel, G., and Kulsrud, R.M. 1975, *Ap.J.*,**201**, 63.

Table 1

Stability properties of an isolated magnetic flux sheet disturbed by convective velocity fluctuations for different plasma $\beta$ and different locations $z_0$ of the lower base of the initial flux sheet.

| $\beta$ | 1 | 1 | 4 | 4 | 4 | 4 | 10 | 10 |
|---|---|---|---|---|---|---|---|---|
| $z_0/H$ | 0 | 5 | -3 | 0 | 3 | 5 | 0 | 5 |
| stability | unstable | unstable | unstable | unstable | unstable | stable | unstable | stable |

## Figure captions

Fig. 1 Numerical results for the case, where $\gamma = 1.05$ (corresponding to the Parker unstable flux sheet), $\beta_0 = 1.0$ and $V_{y0} = 0.9C_s$. (a) the magnetic field lines $\mathbf{B} = (B_x, B_z)$, (b) the density contours ($\log\rho$), (c) the velocity vector $\mathbf{V} = (V_x, V_z)$. Total illustrated area is $(80 \times 35)$ in the unit of H. The contour level step-width is 0.1 for (a) and 0.3 for (b) in the unit of logarithmic scale. The scale of the velocity vector is shown at the top of the figure in (c) in the unit of $C_s$. VNM = 0.67 indicates that the arrow with the length of this line has the velocity of $0.67 \times C_s$. Numbers in the lefthand side of each frame in (a) represent the time in units of $H/C_s$. The solid and dashed curves in (c) at $t = 40$ indicate the positions of intermediate and fast shocks, respectively.

Fig. 2 The distribution in z of (a) the vertical component of velocity $V_z$, (b) the local Alfvén speed $V_a$, (c) the component of magnetic field ($\log B_x$), (d) the component of magnetic field ($\log B_y$), (e) the density ($\log\rho$), (f) the inverse of the local plasma $\beta(= p_g/p_m)$, at $x = X_{max}/2$ (middle of the rising loop) at $t = 27, 34, 43, 46$. The dashed curves in (c) and (e) represent the curves of $\rho \sim \Delta z^{-4}$ and $B_x \sim \Delta z^{-1}$, respectively.

Fig. 3 Time variations of magnetic field lines $\mathbf{B} = (B_x, B_y)$ for the case, where $\gamma = 1.5$ (corresponding to the Parker stable flux sheet) and other parameters are the same as in the model shown in Figure 1. The contour level step-width is 0.05 in units of logarithmic scale. Other remarks are the same as in Figure 1.

Fig. 4 Time variations of magnetic ($E_m$), thermal ($\Delta E_{th}$), kinetic ($\Delta E_k$) and gravitational ($\Delta E_g$) energies contained in the computating domaine, where $\Delta E = E(t) - E(0)$, for the case shown in Fig. 3.

Fig. 5 Time variations of (a) magnetic field lines $\mathbf{B} = (B_x, B_z)$, (b) the density contours ($\log\rho$) and (c) the velocity vector $\mathbf{V} = (V_x, V_z)$ for the case, where $X_{max} = 160H$, $V_{y0} = 3.6C_s$, $w_{sh} = 32H$ and other parameters are the same as in the model shown in Figure 3. Other remarks are the same as in Figure 1.

Fig. 6 The distribution in z of (a) the vertical component of velocity $V_z$, (b) the local Alfvén speed $V_a$, (c) the components of magnetic field ($\log B_x$) and ($\log B_y$), (d) the density ($\log\rho$) at $x = X_{max}/2$ (middle of the rising loop) at $t = 30, 37, 45, 52$.

Fig. 7 Growth rates of the convective instability as a function of horizontal wavenumber for different plasma $\beta$. (a) the case of a partially magnetized convection zone ($z_0 = -2H$), (b) the case of an unmagnetized convective layer ($z_0 = 0$).

Fig. 8 Time evolution of horizontal velocity $V_x$ in the convection zone for the case with $z_0 = -2H$. The dashed line represents the result of the linear stability analysis, the solid line that of the numerical simulations.

Fig. 9 Time variations of the magnetic field lines $\mathbf{B} = (B_x, B_z)$ for the case, where the initial flux sheet is located within the convection zone ($z_0 = -2H$).

Fig. 10 Time variations of the magnetic field lines $\mathbf{B} = (B_x, B_z)$ for the case, where the initial flux sheet is located just above the convectively unstable layer ($z_0 = 0$).

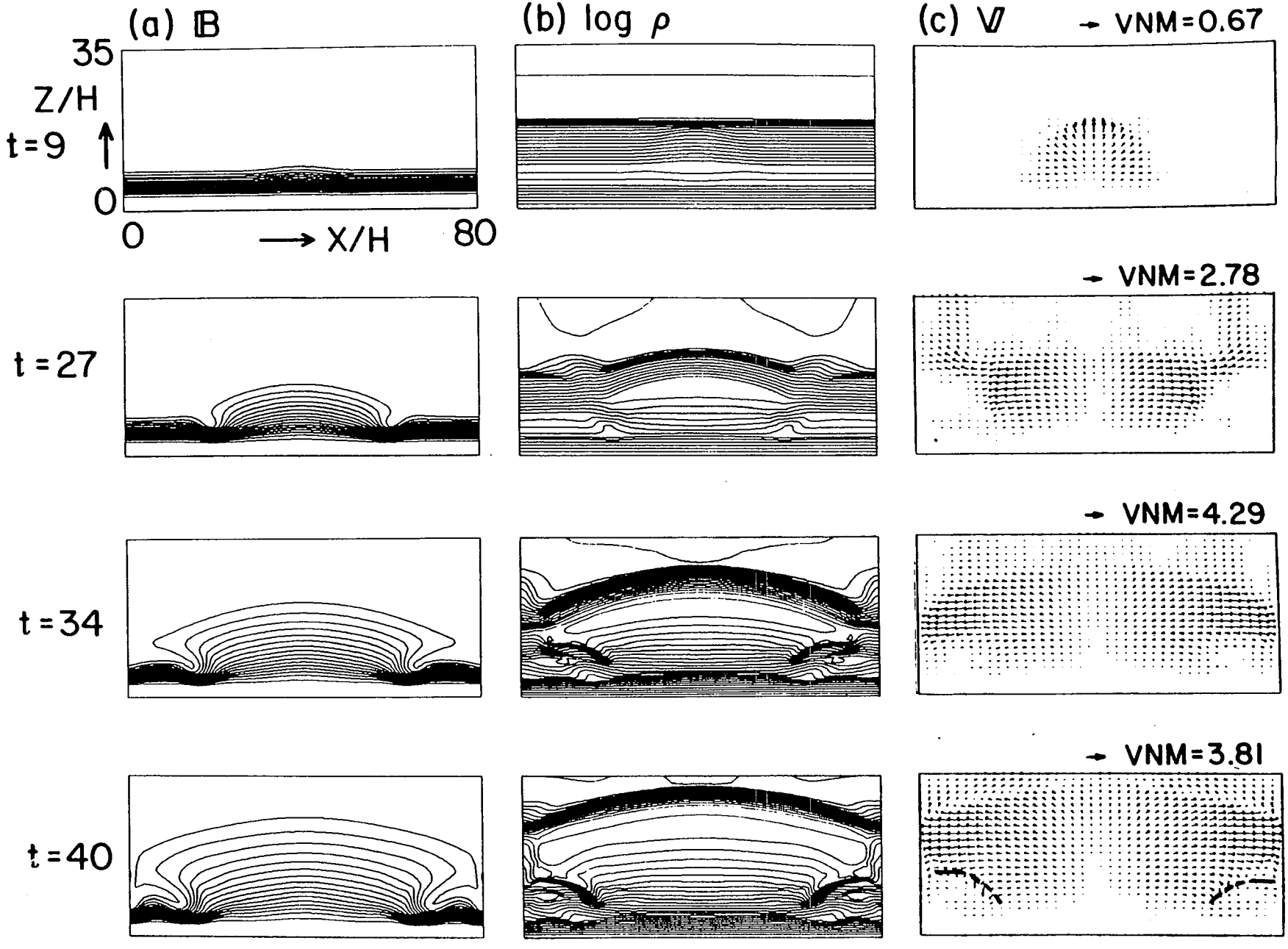
(a) B
(b) log ρ
(c) V
VNM=0.67
35
Z/H
t=9
0
0
X/H
80
VNM=2.78
t=27
VNM=4.29
t=34
VNM=3.81
t=40

Fig. 1

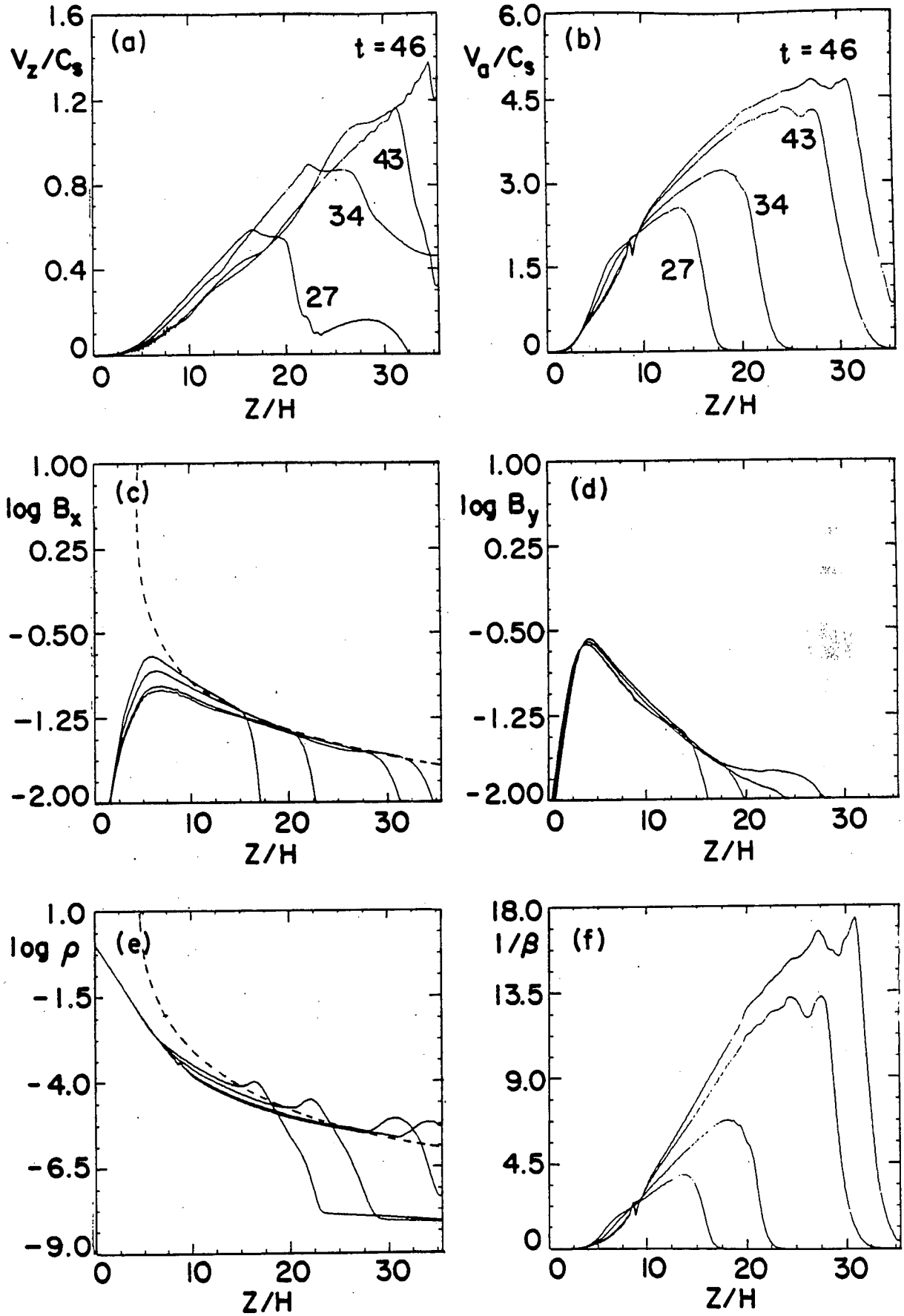
(a)
t = 46
$V_z/C_s$
1.6
1.2
0.8
0.4
0
43
34
27
0
10
20
30
Z/H
(b)
t = 46
$V_a/C_s$
6.0
4.5
3.0
1.5
0
43
34
27
0
10
20
30
Z/H
(c)
log $B_x$
1.00
0.25
-0.50
-1.25
-2.00
0
10
20
30
Z/H
(d)
log $B_y$
1.00
0.25
-0.50
-1.25
-2.00
0
10
20
30
Z/H
(e)
log $\rho$
1.0
-1.5
-4.0
-6.5
-9.0
0
10
20
30
Z/H
(f)
$1/\beta$
18.0
13.5
9.0
4.5
0
0
10
20
30
Z/H

Fig. 2

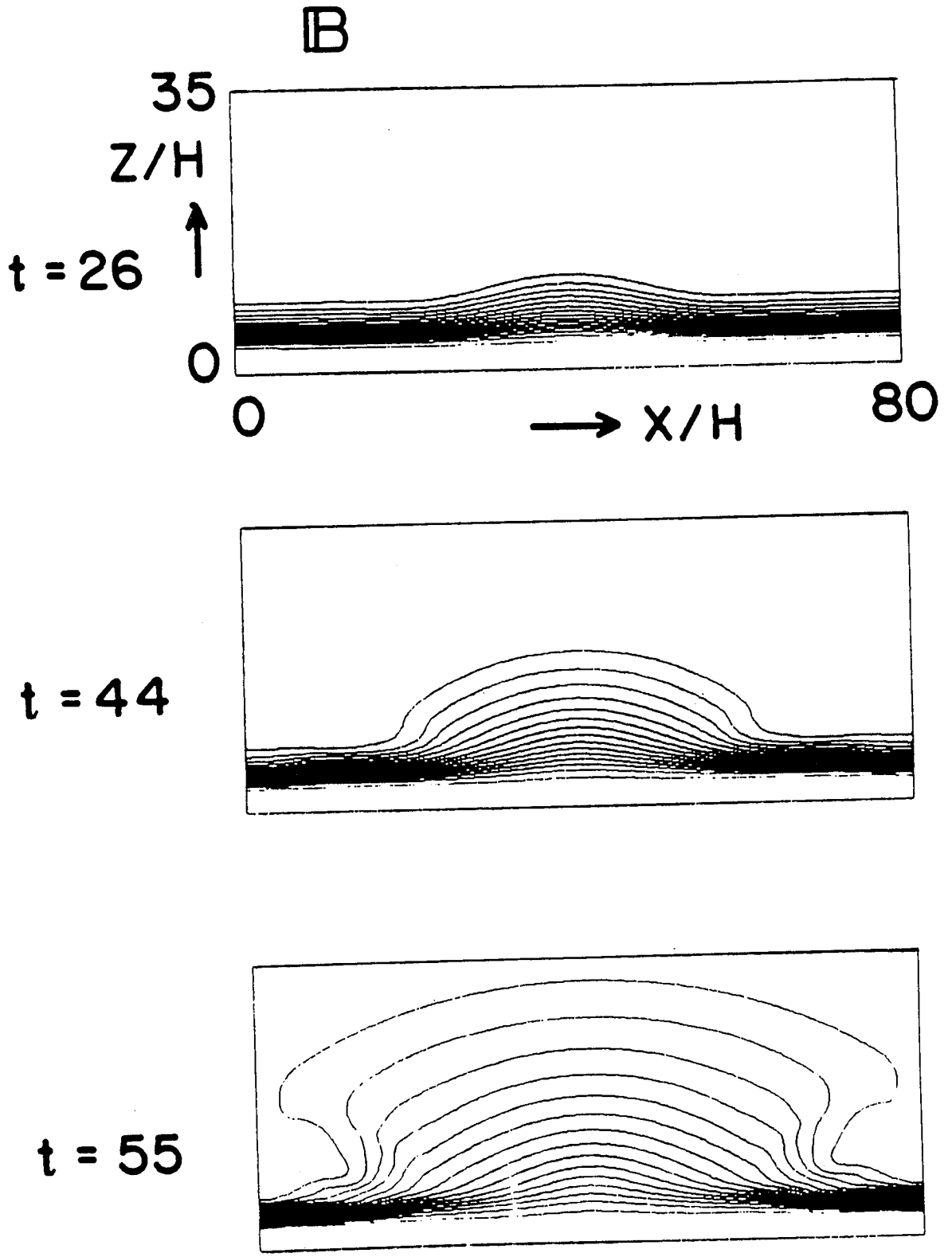


Fig. 3

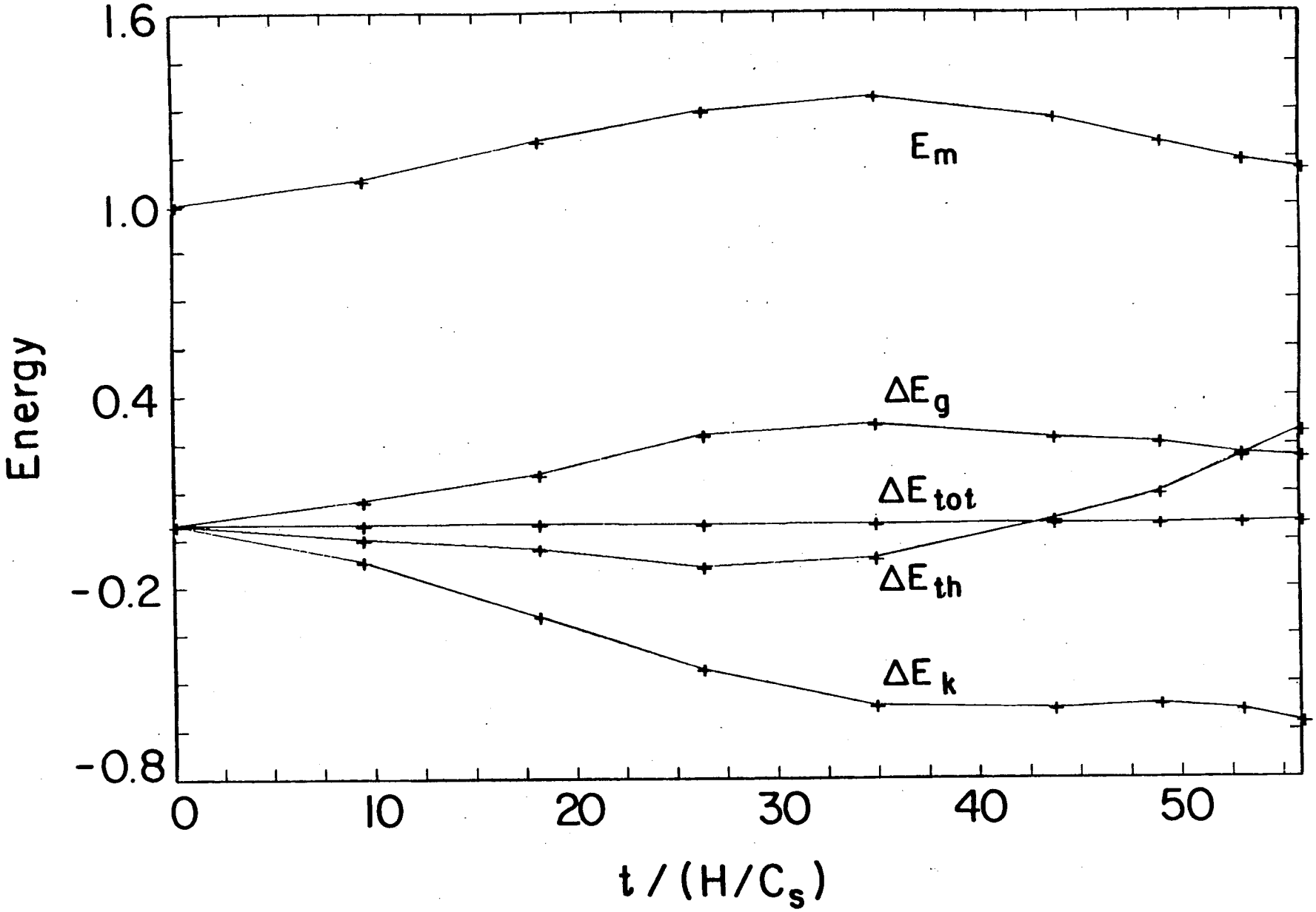


Fig. 4

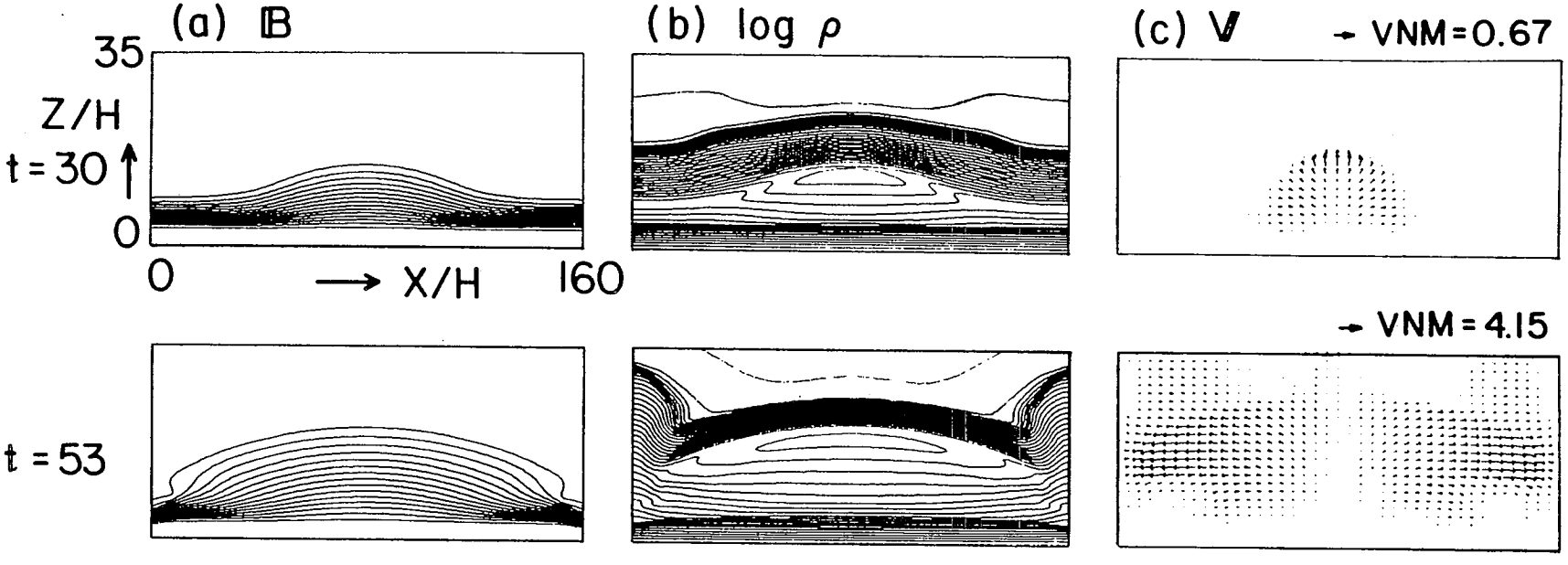


Fig. 5

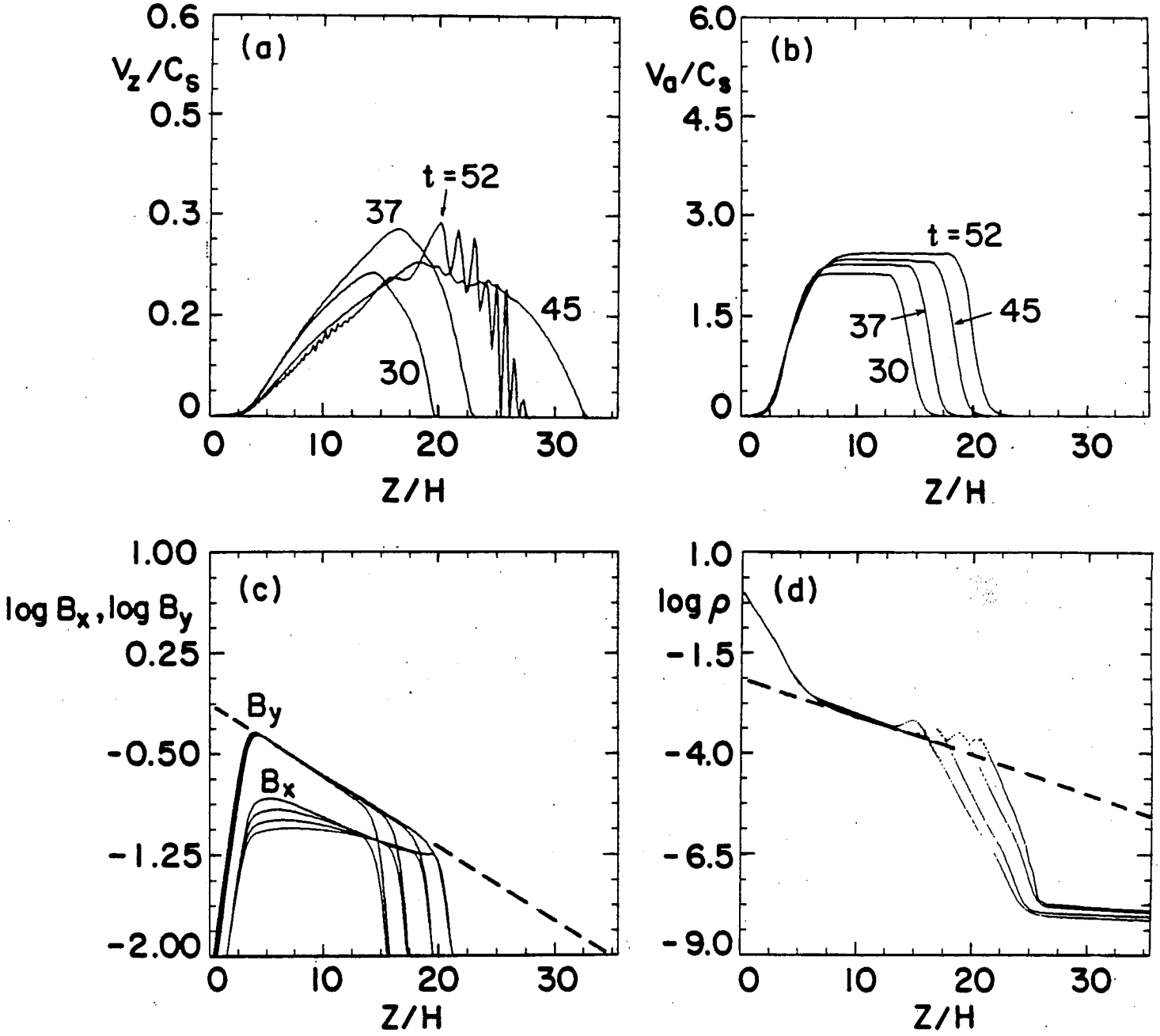
(a)
$V_z/C_s$
0.6
0.5
0.3
0.2
0
t=52
37
45
30
0
10
20
30
Z/H
(b)
$V_a/C_s$
6.0
4.5
3.0
1.5
0
t=52
37
45
30
0
10
20
30
Z/H
(c)
log $B_x$, log $B_y$
1.00
0.25
-0.50
-1.25
-2.00
$B_y$
$B_x$
0
10
20
30
Z/H
(d)
log $\rho$
1.0
-1.5
-4.0
-6.5
-9.0
0
10
20
30
Z/H

Fig. 6

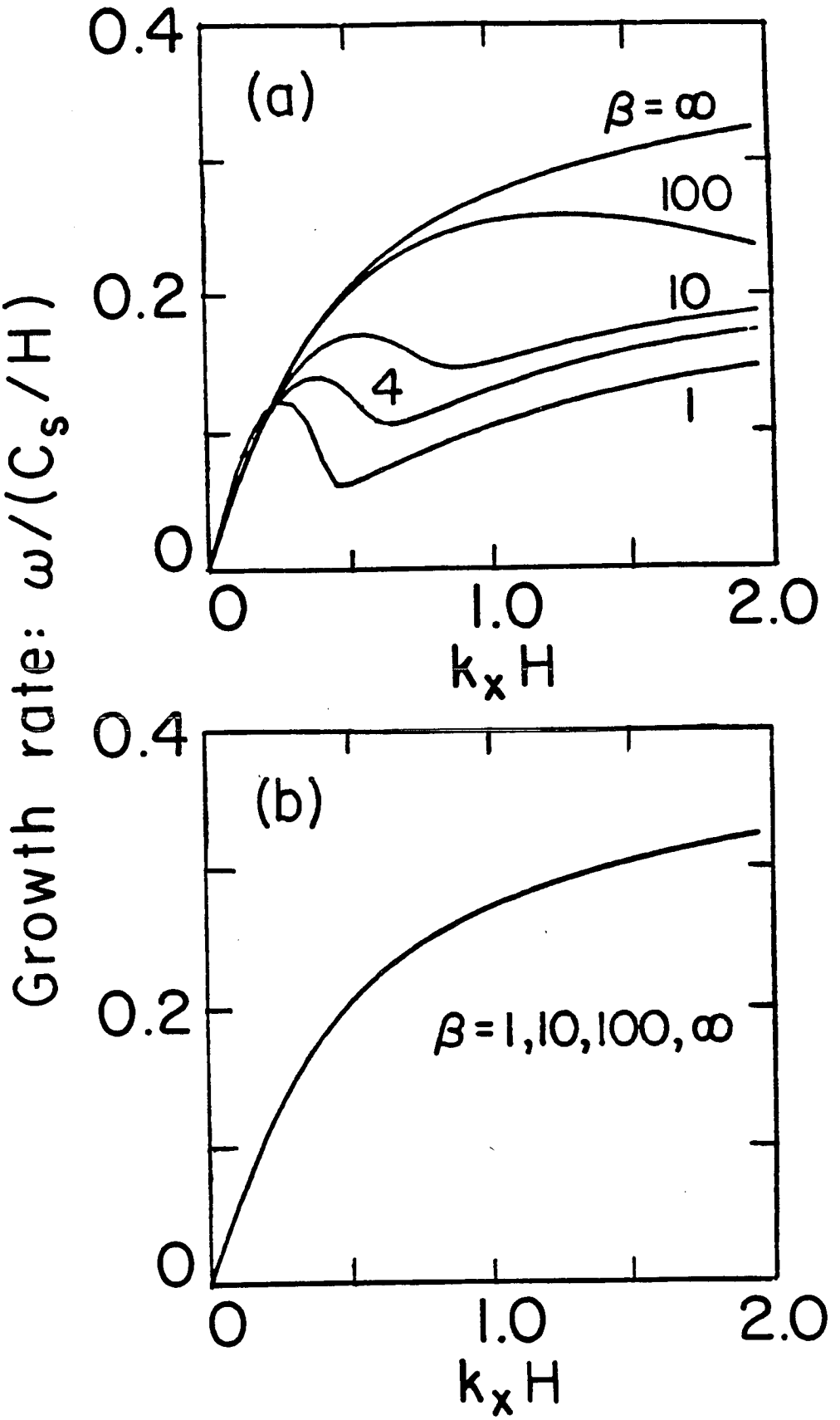
0.4
0.2
0
(a)
β = ∞
100
10
4
1
0
1.0
2.0
k_x H
Growth rate: ω/(C_s/H)
0.4
0.2
0
(b)
β = 1, 10, 100, ∞
0
1.0
2.0
k_x H

Fig. 7

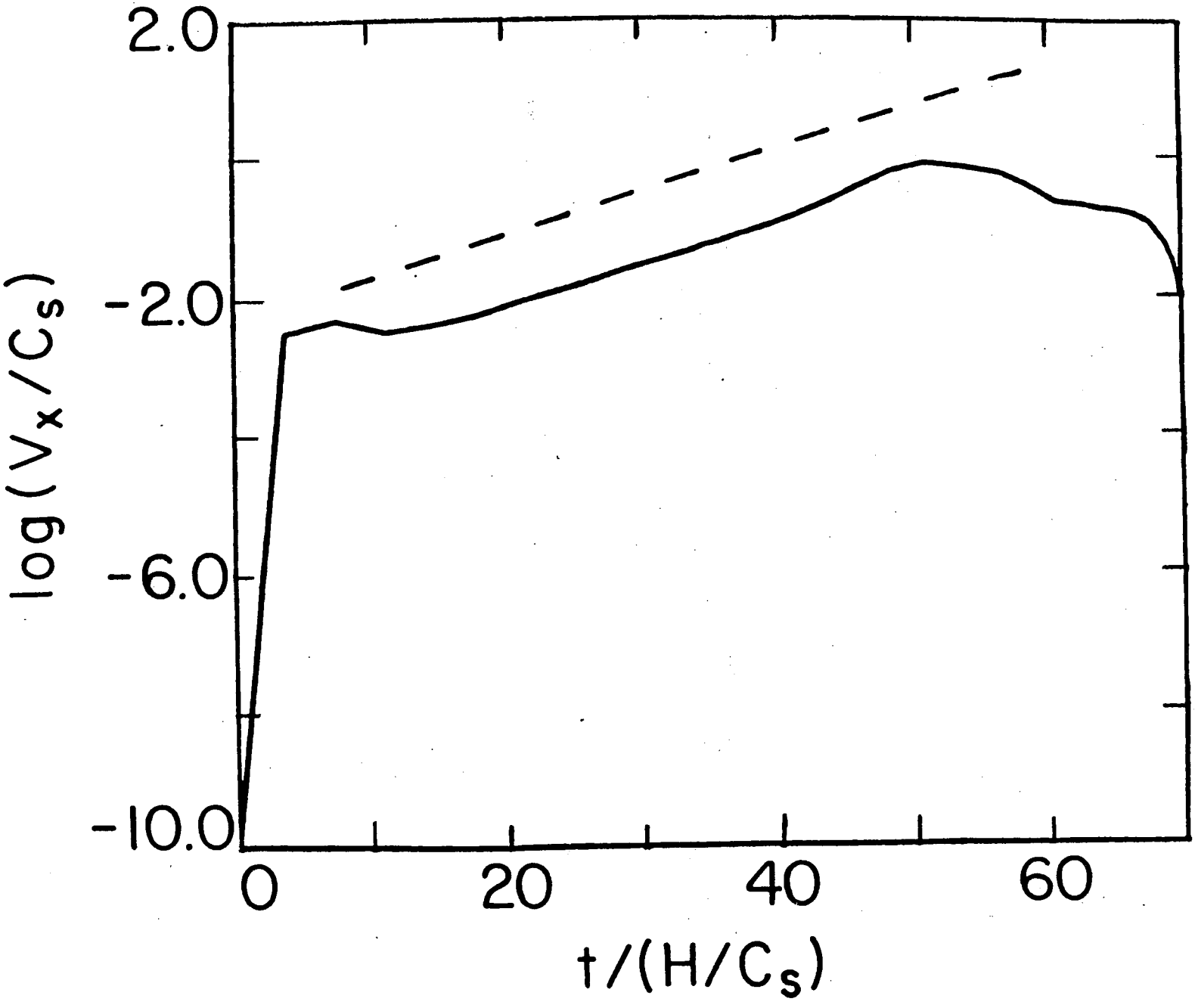


Fig. 8

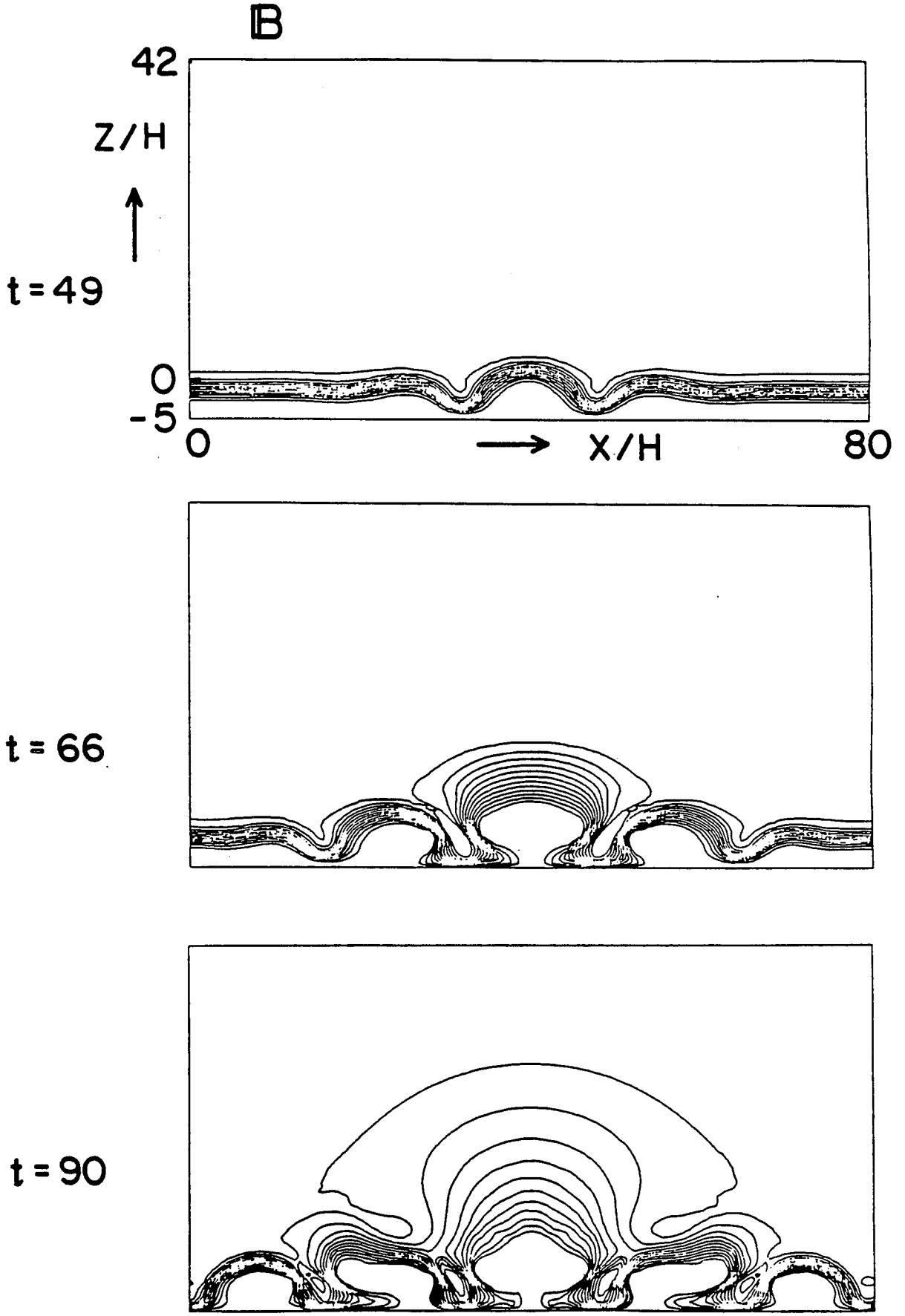


Fig. 9

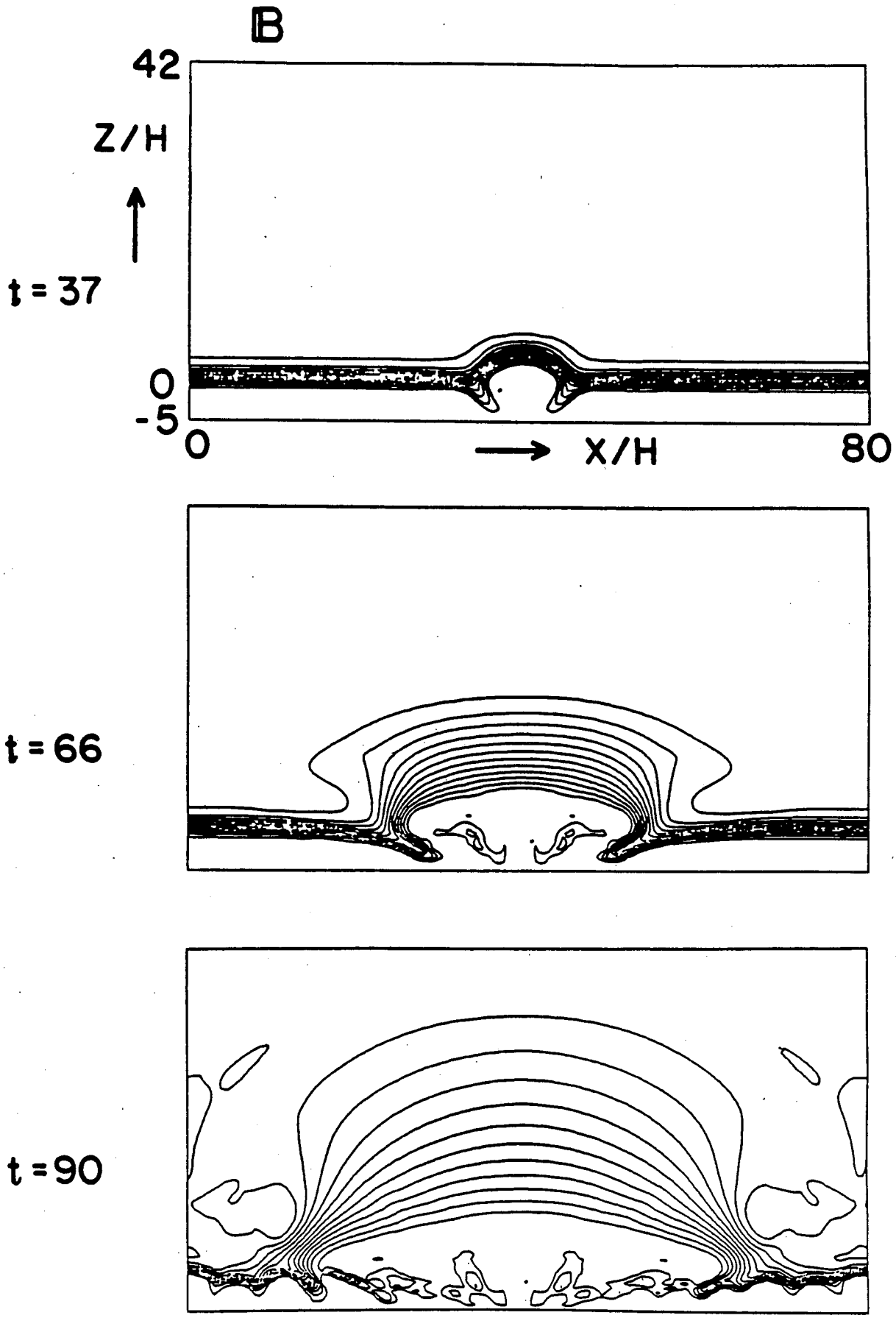


Fig. 10